Available online at www.sciencedirect.com
SCIENCE DIRECT®
ELSEVIER
International Journal of Solids and Structures 43 (2006) 5713–5735
INTERNATIONAL JOURNAL OF SOLIDS and STRUCTURES
www.elsevier.com/locate/ijsolstr

Postbuckling analysis of laminated composite plates subjected to the combination of in-plane shear, compression and lateral loading

Sung-Cheon Han [a,*], Sang-Youl Lee [c], Guillermo Rus [b]

[a] Department of Civil Engineering, Daewon Science College, 599 Shinwol, Jecheon 390-702, Korea
[b] Department of Structural Mechanics, University of Granada, Politécnico de Fuentenueva, 18071 Granada, Spain
[c] Department of Civil Engineering, Hanyang University, 17, Haeongdang-Dong, Seongdong-gu Seoul 133-791, South Korea

Received 9 May 2005
Available online 11 October 2005

Abstract

This study deals with postbuckling behavior of laminated composite plates under the combination of in-plane shear, compression and lateral loading using an Element-based Lagrangian formulation. Natural co-ordinate-based strains, stresses and constitutive equations are used in the present shell element. The Element-based Lagrangian formulation described in this paper, in comparison with the traditional approaches, is more attractive not only because it uses only single mapping but also it converges faster. In addition, the finite element (FE) formulation based on the assumed natural strain method for composite structures shows excellence from the standpoints of computational efficiency as well as its ability to avoid both membrane and shear locking behavior. The numerical results obtained are in good agreement with those reported by other investigators. In particular, new results reported in this paper show the influence of various types of loading, materials and number of layers on postbuckling behavior.

Keywords: Element-based Lagrangian formulation; A 9-node assumed strain shell element; Postbuckling; Laminated composite plates; Combination of in-plane shear and lateral loading

1. Introduction

A new class of materials, fiber-reinforced composite materials, is increasingly being used in a large variety of structures including aerospace, marine and civil infrastructure. With the advancement of technology in fiber-reinforced composite materials, the applicability of composites to such structures has been increased significantly due to their merits such as high strength to weight ratio and resistance to corrosion.

Structural behavior of plates and shells using the finite element method has been studied by a variety of approaches. Ahmad et al. (1970) developed shell elements referred as *degenerate model*. In general, such shell

* Corresponding author. Tel.: +82 43 649 3267; fax: +82 43 649 3555.
E-mail address: techy11@mail.daewon.ac.kr (S.-C. Han).

0020-7683/$ - see front matter © 2005 Elsevier Ltd. All rights reserved.
doi:10.1016/j.ijsolstr.2005.08.004

elements can describe accurately the various behaviors of plates and shells. However, for the thin structures, their performance deteriorates rapidly as the element thickness becomes thin, which is called *shear locking*. In order to overcome the shear locking problems Huang and Hinton (1986) developed a nine-node assumed strain shell element using an enhanced interpolation of the transverse shear strains in the natural coordinate system. Other finite elements employing the assumed strain method were then reported by Jang and Pinsky (1987) independently and also a various background of the assumed strain method was presented by Simo and Hughes (1986). Belytschko et al. (1989) presented a nine-node assumed strain shell element with a stabilized matrix to control the zero energy modes and used a reduced integration for all the terms.

Based on the finite element techniques, various geometrically nonlinear formulations for laminated composite structures are developed in the last two decades. Kim and Voyiadjis (1999) analyzed postbuckling behaviors of laminated composite panels under in-plane compression. Kim et al. (2003) carried out initial buckling and postbuckling analysis of composite plates under pure shear loading. However, the papers on the postbuckling analysis of the laminated composite plates under the combination of in-plane shear, compression and lateral loading have rarely been published. Moreover, most previous studies dealing with composites and isotropic plates subjected to the compressive and combined loading have been limited to elastic buckling behaviors (Featherston and Watson, 2005; Shufrin and Eisenberger, 2005; Featherston, 2003; Loughlan, 2001).

In this paper, to avoid locking phenomena, the assumed natural strain method by Han et al. (2004) is used and the equivalent constitutive equations is used to capture layer effect through the thickness direction. We concentrate on the postbuckling analysis of laminated composite plates under the combination of in-plane shear, compression and lateral loading. For a composite laminate, the combination of various types of loading and lay-up sequences could play a dominant role in determining the nonlinear characteristics. Thus, the study is further extended in this investigation to take into account the effects of loading and stacking sequences. This study uses the first-order shear deformation theory and the numerical results are verified by comparing them with the solutions obtained by Zhang and Matthews (1983a,b, 1985).

2. Geometry of the shell element

In general, the Lagrangian formulations for geometric nonlinear analysis can be classified into two approaches: (1) Total Lagrangian Formulation (TLF), where all the static and kinematic variables are referred back to the initial undeformed configuration ($\mathbf{B}_0$), (2) Updated Lagrangian Formulation (ULF), where all are referred to the current deformed configuration ($\mathbf{B}_t$). Wong (1984) proposed a new variation of Lagrangian formulation known as Element-based Lagrangian Formulation (ELF), where all the static and kinematic variables are referred to a nonphysical "*Element-based*" configuration ($\overline{\mathbf{B}}$) as shown in Fig. 1. Unlike the two traditional Lagrangian formulations, a standard parental element serving as the reference of deformation is to be mapped directly into each element of the initial and deformed configurations in the Element-based Lagrangian Formulation. Therefore, all balance equations governing the deformed configuration can be expressed over the parental element domain in terms of the element natural co-ordinates.

2.1. Initial geometry and kinematic description

The geometry of 9-node shell element shown is Fig. 2 has six degrees of freedom per node. Using the shell assumption of straight normal remaining straight, the initial configuration of the shell element having constant thickness h can be written as

$$\mathbf{P}(\xi_i) = \overline{\mathbf{P}}(\xi_\beta) + \xi_3 \overline{\mathbf{V}}(\xi_\beta), \quad i = 1,2,3, \quad \beta = 1,2, \tag{1}$$

$$\overline{\mathbf{P}}(\xi_\beta) = \sum_{a=1}^{9} N_a(\xi_\beta)\overline{\mathbf{P}}^a, \tag{2}$$

$$\overline{\mathbf{V}}(\xi_\beta) = \sum_{a=1}^{9} N_a(\xi_\beta)\frac{h^a}{2}\widehat{\mathbf{V}}^a, \tag{3}$$

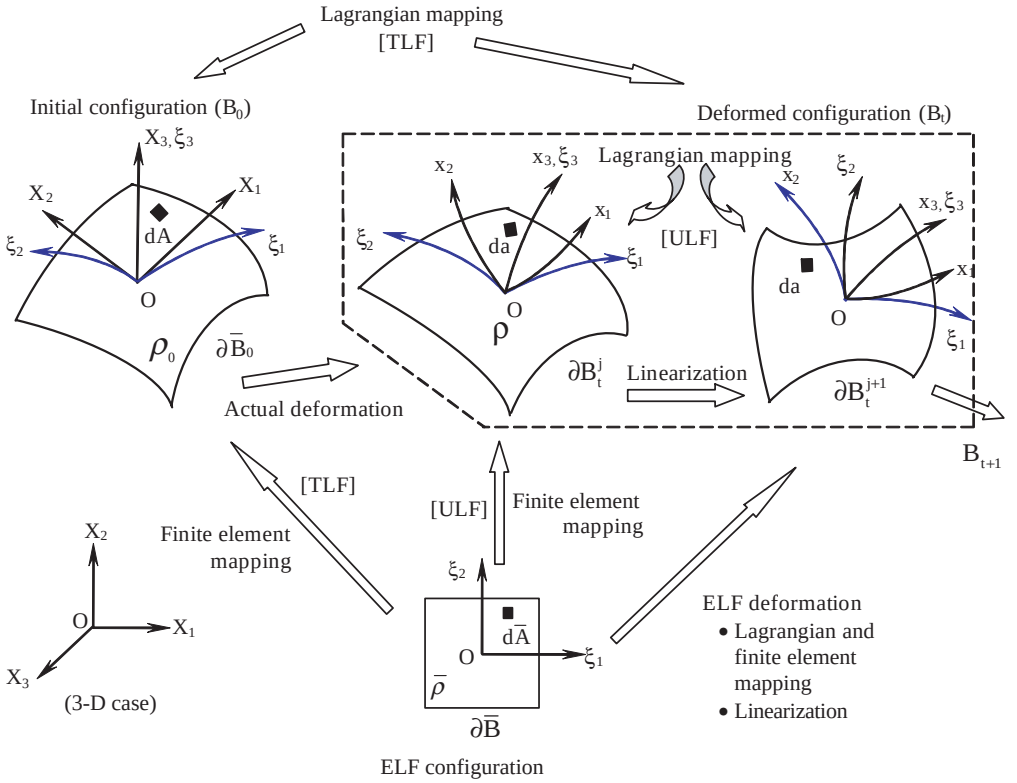

Fig. 1. The element-based Lagrangian formulation method.

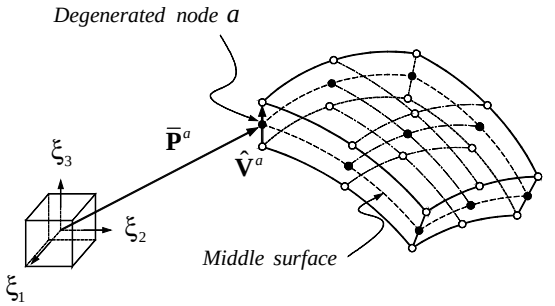

Fig. 2. Geometry of 9-node shell element with six degrees of freedom.

where $\mathbf{P}$ denotes the position vector of a generic point in the shell element; $\overline{\mathbf{P}}$ is the position vector of a point in the mid-surface; N_a denotes the two-dimensional quadratic Lagrangian interpolation function associated with node a; $\overline{\mathbf{P}}^a$ are position vectors which have three Cartesian components; h^a is the thickness of the shell at node a; and $\widehat{\mathbf{V}}^a$ is a unit normal vector at node a, which is normal to the mid-surface. The unit normal vector $\widehat{\mathbf{V}}^a$ at node a can be easily determined by

$$\widehat{\mathbf{V}}^a = \frac{\dfrac{\partial \overline{\mathbf{P}}^a}{\partial \xi_1} \times \dfrac{\partial \overline{\mathbf{P}}^a}{\partial \xi_2}}{\left| \dfrac{\partial \overline{\mathbf{P}}^a}{\partial \xi_1} \times \dfrac{\partial \overline{\mathbf{P}}^a}{\partial \xi_2} \right|}. \tag{4}$$

Finite rotations about the three Cartesian axes, unlike infinitesimal rotations, do not qualify as vectors (Groesberg, 1968). The use of rotations of shell normal about the three global coordinate axes, which is a common practice in linear analysis of shells, has to be abandoned because the transformation and the updating of these rotations require special treatments when finite rotations are involved.

It has been noticed that in the rigid body dynamics, the rotational movement of a rigid body has been dealt with quite successfully by using Euler's angles (Groesberg, 1968), defined by a strict sequence of rotational displacements. The transformation matrix can only represent two independent rotational modes, instead of three modes as required, thus indicating the shortcoming of Euler's angles when small rotation is specialized. In Fig. 3, a new scheme proposed in this study is illustrated, which is based on another strict sequence of three successive rotations. Transformation matrices for these rotations are

$$R_1 = \begin{bmatrix} 1 & 0 & 0 \\ 0 & c_1 & -s_1 \\ 0 & s_1 & c_1 \end{bmatrix}, \qquad R_2 = \begin{bmatrix} c_2 & 0 & s_2 \\ 0 & 1 & 0 \\ -s_2 & 0 & c_2 \end{bmatrix}, \qquad R_3 = \begin{bmatrix} c_3 & -s_3 & 0 \\ s_3 & c_3 & 0 \\ 0 & 0 & 1 \end{bmatrix}, \tag{5}$$

where $c_i = \cos\theta_i$, $s_i = \sin\theta_i$ $(i = 1, 2, 3)$ and the expression of transformation matrix $\mathbf{R}$ is

$$\mathbf{R} = R_1 R_2 R_3 = \begin{bmatrix} c_2 c_3 & -c_2 s_3 & s_2 \\ c_1 s_3 + s_1 s_2 c_3 & c_1 c_3 - s_1 s_2 s_3 & -s_1 c_2 \\ s_1 s_3 - c_1 s_2 c_3 & s_1 c_3 + c_1 s_2 s_3 & c_1 c_2 \end{bmatrix}. \tag{6}$$

The three rotations define a unique transformation matrix $\mathbf{R}$ through Eq. (6); thus they can be used as generalized coordinate for the attached reference system at each node. Then the fibre displacement with respect to the mid-surface will be described by these three rotations. The displacement field $\mathbf{u}$ in the shell element can be defined as

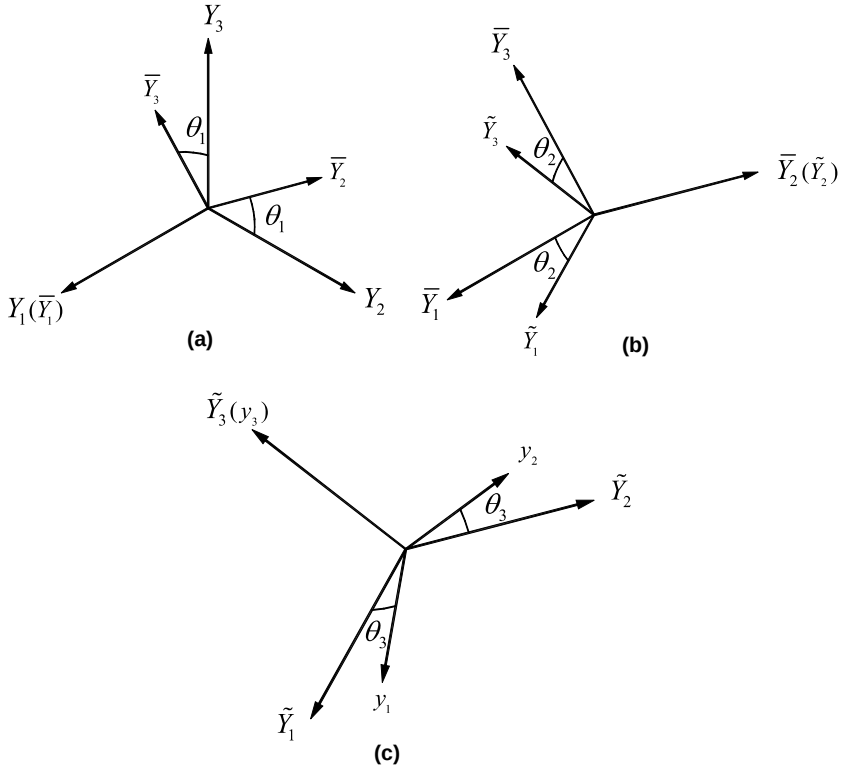

Fig. 3. Proposed rotation expression scheme: (a) a rotation, θ_1, about Y_1 axis; (b) a rotation, θ_2, about $\overline{Y}_2$ axis; (c) a rotation, θ_3, about $\tilde{Y}_3$ axis.

$$\mathbf{u}(\xi_i) = \sum_{a=1}^{9} N_a(\xi_\beta)\left[\bar{\mathbf{u}}^a + \xi_3 \frac{h^a}{2}\widehat{\mathbf{e}}^a\right] = \bar{\mathbf{u}}(\xi_\beta) + \xi_3 \bar{\mathbf{e}}(\xi_\beta), \tag{7}$$

where $\bar{\mathbf{u}}$ is the transitional displacement vector of a point in the mid-surface and $\widehat{\mathbf{e}}^a$ is the fibre displacement vector at the node a, i.e.,

$$\hat{\mathbf{e}}^a = \mathbf{R}^a \widehat{\mathbf{V}}^a - \widehat{\mathbf{V}}^a. \tag{8}$$

Consequently, using Eq. (8), the displacement field in Eq. (7) can be expressed as

$$\mathbf{u}(\xi_i) = \sum_{a=1}^{9} N_a(\xi_\beta)\left[\bar{\mathbf{u}}^a + \xi_3 \frac{h^a}{2}(\mathbf{R}^a - \mathbf{I}_{3\times 3})\widehat{\mathbf{V}}^a\right], \tag{9}$$

where $\mathbf{I}_{3\times 3}$ is a unit matrix.

2.2. Incremental rotational and displacement vector

We first refer to the angular velocity vector in the analytical mechanics. It is well known that angular velocity is a vector, although its components are non-integrable (Meirovitch, 1970). Now that geometrically nonlinear problems with large rotations are solved by iterative methods, the incremental rotations have to be dealt with appropriately (Fig. 4). The incremental rotations may be regarded as small when the displacement fields are linearized and therefore can be treated as vectors like the angular velocity. Given a set of incremental rotations $\Delta\theta_1$, $\Delta\theta_2$ and $\Delta\theta_3$, an incremental rotation vector is defined as

$$\Delta\mathbf{r} = \Delta\mathbf{r}_1 + \Delta\mathbf{r}_2 + \Delta\mathbf{r}_3, \tag{10}$$

where

$$\Delta\mathbf{r}_1 = \Delta\theta_1\boldsymbol{\varphi}_1, \quad \Delta\mathbf{r}_2 = \Delta\theta_2\boldsymbol{\varphi}_2, \quad \Delta\mathbf{r}_3 = \Delta\theta_3\boldsymbol{\varphi}_3 \tag{11}$$

with $\boldsymbol{\varphi}_1$, $\boldsymbol{\varphi}_2$ and $\boldsymbol{\varphi}_3$ representing unit vectors along the directions of axes Y_1, $\overline{Y}_2$ and $\widetilde{Y}_3(y_3)$, respectively.

This incremental rotation vector can be expressed in different reference systems:

(a) In the fixed global coordinate system $x_1x_2x_3$

$$\Delta\mathbf{r} = \begin{Bmatrix} \Delta\theta_{x_1} \\ \Delta\theta_{x_2} \\ \Delta\theta_{x_3} \end{Bmatrix} = R_G \begin{Bmatrix} \Delta\theta_1 \\ \Delta\theta_2 \\ \Delta\theta_3 \end{Bmatrix}, \tag{12}$$

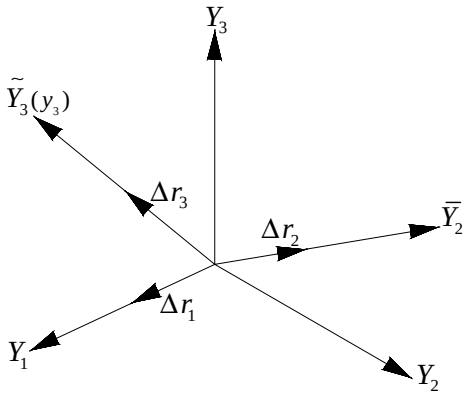

Fig. 4. Incremental rotation vector.

where

$$R_G = \begin{bmatrix} 1 & 0 & s_2 \\ 0 & c_1 & -s_1 c_2 \\ 0 & s_1 & c_1 c_2 \end{bmatrix}. \tag{13}$$

(b) In the attached reference system $y_1 y_2 y_3$

$$\Delta\bar{\mathbf{r}} = \begin{Bmatrix} \Delta\theta_{y_1} \\ \Delta\theta_{y_2} \\ \Delta\theta_{y_3} \end{Bmatrix} = \mathbf{R}^{\mathrm{T}} \Delta\mathbf{r} = R_A \begin{Bmatrix} \Delta\theta_1 \\ \Delta\theta_2 \\ \Delta\theta_3 \end{Bmatrix}, \tag{14}$$

where

$$R_A = \mathbf{R}^{\mathrm{T}} R_G = \begin{bmatrix} c_2 c_3 & s_3 & 0 \\ -c_2 s_3 & c_3 & 0 \\ s_2 & 0 & 1 \end{bmatrix}. \tag{15}$$

For node a, the increment of the nodal fiber displacement in the attached reference system due to the incremental normal rotation $\Delta\bar{\mathbf{r}}^a$, can be expressed as

$$\Delta\hat{\mathbf{e}}_A^a = \left(\frac{\xi_3 h^a}{2}\right)\left(\Delta\bar{\mathbf{r}}^a \times \widehat{\mathbf{V}}^a\right) = \left(\frac{\xi_3 h^a}{2}\right)\mathbf{\Psi}^a \begin{Bmatrix} \Delta\bar{\mathbf{r}}_1 \\ \Delta\bar{\mathbf{r}}_2 \\ \Delta\bar{\mathbf{r}}_3 \end{Bmatrix}^a \tag{16}$$

in which

$$\mathbf{\Psi}^a = \begin{bmatrix} 0 & \widehat{V}_3^a & -\widehat{V}_2^a \\ -\widehat{V}_3^a & 0 & \widehat{V}_1^a \\ \widehat{V}_2^a & -\widehat{V}_1^a & 0 \end{bmatrix}. \tag{17}$$

Thus, the increment of nodal fiber displacement due to the incremental rotation of normal can be expressed in the global reference system as

$$\Delta\hat{\mathbf{e}}^a(\xi_3) = \mathbf{R}^a \Delta\hat{\mathbf{e}}_A^a(\xi_3) = \left(\frac{\xi_3 h^a}{2}\right)\mathbf{R}^a \mathbf{\Psi}^a \Delta\bar{\mathbf{r}}^a \tag{18}$$

which can be written in the form

$$\Delta\hat{\mathbf{e}}^a(\xi_3) = \xi_3 \mathbf{H}^a \begin{Bmatrix} \Delta\theta_1 \\ \Delta\theta_2 \\ \Delta\theta_3 \end{Bmatrix}^a, \tag{19}$$

where

$$\mathbf{H}^a = \frac{h^a}{2}\mathbf{R}^a \mathbf{\Psi}^a R_A^a. \tag{20}$$

Let the nodal incremental displacement vector for node a be

$$\Delta\mathbf{U}^a = \left\{\Delta\bar{u}_1^a, \Delta\bar{u}_2^a, \Delta\bar{u}_3^a, \Delta\theta_1^a, \Delta\theta_2^a, \Delta\theta_3^a\right\}^{\mathrm{T}}. \tag{21}$$

The increment of nodal fiber displacement will be

$$\Delta\mathbf{u}^a(\xi_3) = [\mathbf{I}_{3x3} | \xi_3 \mathbf{H}^a] \Delta\mathbf{U}^a. \tag{22}$$

Then the incremental displacement field within the element can be expressed as

$$\Delta\mathbf{u}(\xi_i) = \sum_{a=1}^{9} N_a(\xi_\beta) \Delta\mathbf{u}^a(\xi_3) = \sum_{a=1}^{9} N_a(\xi_\beta) [\mathbf{I}_{3\times 3} | \xi_3 \mathbf{H}^a] \Delta\mathbf{U}^a. \tag{23}$$

3. Torsional effect

As the element has no direct stiffness contribution to the drilling degree of freedom, the stiffness matrix may be singular if neighboring elements are nearly co-plane. In the past, a fictitious torsional spring was added either locally at the element level, or in some pseudo-normal direction defined at each node. This technique often is found unsatisfactory, especially for a flexible system in which an unrealistic amount of strain energy in the spring can be produced by a rigid body motion. In this study, based on the procedure proposed by Kanok-Nukulchai (1979), the drilling degree of freedom will be tied to the in-plane twist by a penalty functional through an additional strain energy as

$$U_t = k_t G \int_{V^e} \left[\alpha_t(\xi_1, \xi_2) - \frac{1}{2} \left\{ \frac{\partial w_2}{\partial z_1}(\xi_1, \xi_2, 0) - \frac{\partial w_1}{\partial z_2}(\xi_1, \xi_2, 0) \right\} \right]^2 \mathrm{d}V, \tag{24}$$

where k_t is a parameter to be determined (the value of 0.1 is suggested); G is the shear modulus; V^e is the volume of the element; α_t is the in-plane torsional rotation; w_1 and w_2 are displacement components in the local coordinate system; z_i ($i = 1, 2, 3$) are local Cartesian coordinates with z_3 axis normal to the shell mid-surface; and $\mathrm{d}V$ is the volume element. A two-by-two Gauss integration scheme is applied for the evaluation of the torsional stiffness in order to avoid the over-constrained situation.

4. Natural strain tensor

Following the natural co-ordinate system (Han et al., 2004), the natural strain tensor corresponding to the Green strain tensor may be defined as

$$\widetilde{E}_{\alpha\beta} = \frac{\partial \mathbf{P}_I}{\partial \xi_\alpha} \frac{\partial \mathbf{P}_J}{\partial \xi_\beta} E_{IJ}. \tag{25}$$

It should be noted that the Green strain tensor and the natural strain have the following tensor transformation relationship

$$\widetilde{E}_{\alpha\beta} = \frac{1}{2} \left[\frac{\partial \mathbf{P}_I}{\partial \xi_\alpha} \frac{\partial \mathbf{u}_I}{\partial \xi_\beta} + \frac{\partial \mathbf{u}_J}{\partial \xi_\alpha} \frac{\partial \mathbf{P}_J}{\partial \xi_\beta} \right]. \tag{26}$$

The incremental membrane, bending and transverse shear strains with Eq. (26) can be separated into linear and nonlinear parts such as:

$$\Delta\widetilde{E}^m = \Delta^L\widetilde{E}^m + \Delta^{NL}\widetilde{E}^m, \tag{27a}$$

$$\Delta\widetilde{E}^b = \Delta^L\widetilde{E}^b + \Delta^{NL}\widetilde{E}^b, \tag{27b}$$

$$\Delta\widetilde{E}^s = \Delta^L\widetilde{E}^s + \Delta^{NL}\widetilde{E}^s. \tag{27c}$$

5. Strain energy and stress resultants of laminated plates

The strain energy U of the shell represented as a three-dimensional body is given by the expression, where in curvilinear coordinates the stress tensor S_{ij} is contracted with the strain tensor E_{ij}

$$U = \frac{1}{2} \int_V S_{ij} E_{ij} \, \mathrm{d}V. \tag{28}$$

In the laminated structures, the stiffness properties are function of the normal coordinate. In Fig. 5, a cross-section of laminated plate composed of N layers is presented. A linear elastic properties of the anisotropic layers are characterized by the tensor of elasticity C_{ijkl}. In many applications, it can be assumed that calculations of shell stiffness properties can be performed neglecting the differences in spatial and shell mid-surface metrics. In this case, the Hook's law for each layer can be written by

$$S_{ij} = C_{ijkl} E_{kl}. \tag{29}$$

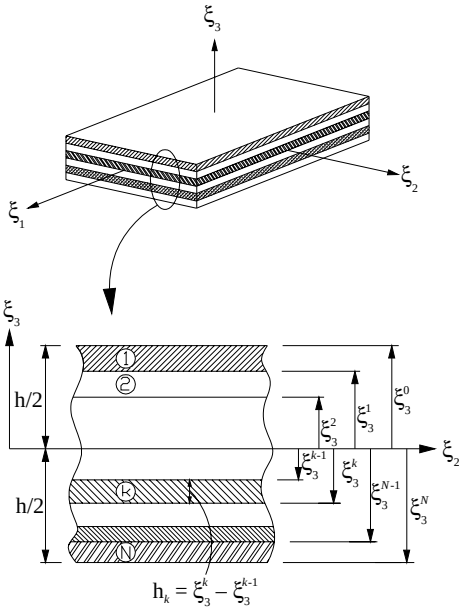

Fig. 5. Cross-section of laminated plate composed of N layers.

Since the present formulation is based on the natural co-ordinate reference frame, we introduce here an explicit transformation scheme between natural co-ordinates and the global co-ordinate system, to obtain a natural co-ordinate based constitutive equation (Kim and Park, 2002; Kim et al., 2003). The stress tensor in the natural coordinate can be written as follows:

$$\widetilde{S}_{ij} = \widetilde{C}_{ijkl}\widetilde{E}_{kl} = \widetilde{J}_0 \mathbf{T}\widetilde{D}_{ijkl}\mathbf{T}^{\mathrm{T}}\widetilde{E}_{kl}, \tag{30}$$

where $\widetilde{J}_0$ is the determinant of the Jacobian matrix and $\widetilde{D}_{ijkl}$ is the constitutive matrix for orthotropic materials with the material angle θ. The transformation matrix $\mathbf{T}$ in Eq. (30) is given by Han et al. (2004). Substituting Eq. (30) into Eq. (28) the strain energy U can be expressed by

$$U = \frac{1}{2}\int_A \int_{-h/2}^{h/2} \widetilde{C}_{ijkl}\widetilde{E}_{ij}\widetilde{E}_{kl}\,\mathrm{d}\xi_3\,\mathrm{d}A. \tag{31}$$

After integration, throughout the thickness, the strain energy can be obtained in terms of shell quantities: stress resultants and couples and laminated shell stiffness characteristics

$$\begin{aligned} A_{\alpha\beta\gamma\delta}, B_{\alpha\beta\gamma\delta}, D_{\alpha\beta\gamma\delta} &= \int_{-h/2}^{h/2} \widetilde{C}_{\alpha\beta\gamma\delta}(1, \xi_3, \xi_3^2)\,\mathrm{d}\xi_3, \\ A_{\alpha 3\beta 3} &= k_s \int_{-h/2}^{h/2} \widetilde{C}_{\alpha 3\beta 3}\,\mathrm{d}\xi_3. \end{aligned} \tag{32}$$

The Reissner's value of 5/6 is used as the transverse shear correction factor (k_s) in the FE formulation based on the first shear deformation theory.

The shell element displays resultant forces acting on a laminate which are obtained by integration of stresses through the laminate thickness. In this study, we impose the plane state on the natural constitutive equation of Eq. (30) before forming the equivalent constitutive equation. The constitutive relations of the composite laminate are as follows:

$$\begin{Bmatrix} N_{\alpha\beta} \\ M_{\alpha\beta} \\ Q_{\alpha 3} \end{Bmatrix} = \begin{bmatrix} A_{\alpha\beta\gamma\delta} & B_{\alpha\beta\gamma\delta} & 0 \\ B_{\alpha\beta\gamma\delta} & D_{\alpha\beta\gamma\delta} & 0 \\ 0 & 0 & A_{\alpha 3\beta 3} \end{bmatrix} \begin{Bmatrix} \widetilde{E}^{m}_{\gamma\delta} \\ \widetilde{E}^{b}_{\gamma\delta} \\ \widetilde{E}^{s}_{\beta 3} \end{Bmatrix}. \tag{33}$$

6. Transverse shear and membrane locking

In order to avoid locking problems, the assumed natural strain method in the nine-node shell element by Han et al. (2004) is used. Thus the transverse shear and membrane strain fields are interpolated with the following sampling points,

$$\begin{aligned} \tilde{e}_{13} &= \sum_{i=1}^{2}\sum_{j=1}^{3} \Omega_i(\xi_1)\Xi_j(\xi_2)\widetilde{E}^{\delta}_{13}, \quad \tilde{e}_{23} = \sum_{i=1}^{2}\sum_{j=1}^{3} \Omega_i(\xi_2)\Xi_j(\xi_1)\widetilde{E}^{\delta}_{23}, \\ \tilde{e}_{12} &= \sum_{i=1}^{2}\sum_{j=1}^{2} \Omega_i(\xi_1)\Omega_j(\xi_2)\widetilde{E}^{\delta}_{12}, \end{aligned} \tag{34}$$

where $\delta = 2(j-1)+i$ denotes the position of the sampling point as shown in Fig. 6 and the shape function $\Omega_i(\xi_1)$ and $\Xi_j(\xi_2)$ are

$$\begin{aligned} &\Omega_1(\xi_1) = \frac{1}{2}(1+\sqrt{3}\xi_1), \quad \Omega_2(\xi_1) = \frac{1}{2}(1-\sqrt{3}\xi_1), \\ &\Xi_1(\xi_2) = \frac{1}{2}\xi_2(\xi_2+1), \quad \Xi_2(\xi_2) = 1-\xi_2^2, \quad \Xi_3(\xi_2) = \frac{1}{2}\xi_2(\xi_2-1) \end{aligned} \tag{35}$$

in which $\Omega_i(\xi_2)$ and $\Xi_i(\xi_1)$ can be obtained by changing variables. The assumed strain $\tilde{e}_{11}$, $\tilde{e}_{22}$ have the same interpolation scheme as $\tilde{e}_{13}$, $\tilde{e}_{23}$, respectively.

The assumed strains $\tilde{e}$ derived from Eq. (34) are used in the present shell element instead of the strains $\widetilde{E}$ of Eq. (26) obtained from the displacement field. In this study, a $\widetilde{\mathbf{B}}_{\mathbf{AS}}$ matrix was implemented from assumed natural strains instead of using the standard $\widetilde{\mathbf{B}}$ matrix as shown in Eq. (36).

$$\begin{Bmatrix} \tilde{e}^{m} \\ \widetilde{E}^{b} \\ \tilde{e}^{s} \end{Bmatrix} = \begin{bmatrix} (\widetilde{\mathbf{B}}_{\mathbf{m}})_{\mathbf{AS}} & 0 \\ \xi_3\widetilde{\mathbf{B}}_{\mathbf{b1}} & \xi_3\widetilde{\mathbf{B}}_{\mathbf{b2}} \\ (\widetilde{\mathbf{B}}_{\mathbf{s1}})_{\mathbf{AS}} & (\widetilde{\mathbf{B}}_{\mathbf{s2}})_{\mathbf{AS}} \end{bmatrix} \begin{Bmatrix} \bar{\mathbf{u}} \\ \boldsymbol{\theta} \end{Bmatrix}, \tag{36}$$

where $\tilde{e}^{m}$ and $\tilde{e}^{s}$ are assumed membrane and assumed transverse shear strain components.

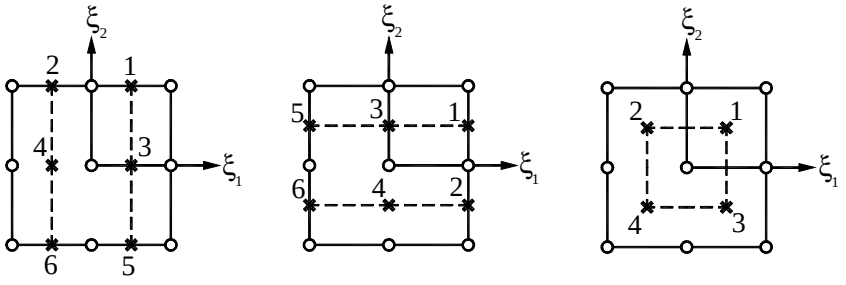

Fig. 6. Sampling points for assumed strains of $\tilde{e}_{11}$, $\tilde{e}_{13}$, $\tilde{e}_{22}$, $\tilde{e}_{23}$ and $\tilde{e}_{12}$.

7. Incremental equation of equilibrium

The generalized Hook's law at large strain does not represent an approximate material behavior description because stress-strain relation is non-linear. From the practical point of view, Hook's law is only applicable to small strain, which constitutive tensor is constant coefficient. Using small strain assumption, the following incremental equilibrium equation is obtained.

$$\int \delta(\Delta^L \widetilde{E})^{\mathrm{T}} \widetilde{\mathbf{C}} \Delta^L \widetilde{E} \, \mathrm{d}V + \int \mathbf{S}(\Delta^{NL} \widetilde{E}) \, \mathrm{d}V = {}^{t+\Delta t}\delta W_{\mathrm{ext}} - \int \delta(\Delta^L \widetilde{E})^{\mathrm{T}} \mathbf{S} \, \mathrm{d}V, \tag{37}$$

where superscript t which is generally used as the current configuration is ignored in the above Eq. (37) and superscript $t+\Delta t$ is the adjust incremented configuration, ${}^{t+\Delta t}\delta W_{\mathrm{ext}}$ is the external virtual work in $t+\Delta t$.

The total tangent stiffness comprises the material stiffness and the geometric stiffness. The linear part of the Green strain tensor is used to derive the material stiffness matrix and non-linear part of the Green strain tensor is used to derive the geometric stiffness matrix.

7.1. Material stiffness matrix

If the strain-displacement Eq. (27) is substituted into Eq. (37), the linearized element material stiffness matrix ($\mathbf{K_L}$) is obtained.

$$\int \delta(\Delta^L \widetilde{E})^{\mathrm{T}} \widetilde{\mathbf{C}} \Delta^L \widetilde{E} \, \mathrm{d}V = \delta \Delta \mathbf{U}^{\mathbf{T}} \left(\int \widetilde{\mathbf{B}}^{\mathbf{T}} \widetilde{\mathbf{C}} \widetilde{\mathbf{B}} \, \mathrm{d}V \right) \Delta \mathbf{U} = \delta \Delta \mathbf{U}^{\mathbf{T}} \mathbf{K_L} \Delta \mathbf{U}. \tag{38}$$

For laminated composite structures, the stress resultant form which is called the equivalent constitutive equations as derived in Eq. (33) are used to capture layer effect through the thickness direction. The element stiffness matrix may be written in a matrix form using the equivalent constitutive equations. Finally the element stiffness matrix has 6×6 size on the reference-surface of shell element.

$$[\mathbf{K_L}] = \int \begin{bmatrix} \mathbf{K_L^{11}} \mathbf{K_L^{12}} \\ \mathbf{K_L^{21}} \mathbf{K_L^{22}} \end{bmatrix}_{6\times 6} \mathrm{d}A, \tag{39}$$

where the sub-matrix of $[\mathbf{K_L}]$ is shown in Han et al. (2004).

7.2. Geometric stiffness matrix

In order to obtain an accurate geometric stiffness matrix, the stresses should be evaluated accurately. The accuracy of the computation of stresses for formulation of geometric stiffness matrix is maintained by obtaining the same interpolated strains in the computation of linear stiffness matrix. The stresses are computed at the integration points based on these strains. Ignoring the second order term ξ_3^2 in Eq. (27), the following relation is obtained.

$$\{{}^{NL}\widetilde{E}_{\alpha\beta}\} = \begin{Bmatrix} {}^{NL}\widetilde{E}_{11} \\ {}^{NL}\widetilde{E}_{22} \\ 2{}^{NL}\widetilde{E}_{12} \\ 2{}^{NL}\widetilde{E}_{23} \\ 2{}^{NL}\widetilde{E}_{13} \end{Bmatrix} = \frac{1}{2} \begin{bmatrix} \frac{\partial u_I}{\partial \xi_1} & 0 & 0 \\ 0 & \frac{\partial u_I}{\partial \xi_2} & 0 \\ \frac{\partial u_I}{\partial \xi_2} & \frac{\partial u_I}{\partial \xi_1} & 0 \\ 0 & \frac{\partial u_I}{\partial \xi_3} & \frac{\partial u_I}{\partial \xi_2} \\ \frac{\partial u_I}{\partial \xi_3} & 0 & \frac{\partial u_I}{\partial \xi_1} \end{bmatrix} \begin{bmatrix} \frac{\partial u_I}{\partial \xi_1} \\ \frac{\partial u_I}{\partial \xi_2} \\ \frac{\partial u_I}{\partial \xi_3} \end{bmatrix} = \frac{1}{2} \mathbf{Q} \Omega. \tag{40}$$

The each component of displacement gradient can be expressed as follows:

$$\frac{\partial u_I}{\partial \xi_1} = \begin{Bmatrix} \frac{\partial u_1}{\partial \xi_1} \\ \frac{\partial u_2}{\partial \xi_1} \\ \frac{\partial u_3}{\partial \xi_1} \end{Bmatrix} = \begin{bmatrix} \frac{\partial}{\partial \xi_1} & & \\ & \frac{\partial}{\partial \xi_1} & \\ & & \frac{\partial}{\partial \xi_1} \end{bmatrix} \begin{Bmatrix} \bar{u}_1 \\ \bar{u}_2 \\ \bar{u}_3 \end{Bmatrix} + \xi_3 \begin{bmatrix} \frac{\partial}{\partial \xi_1} & & \\ & \frac{\partial}{\partial \xi_1} & \\ & & 0 \end{bmatrix} \begin{Bmatrix} \bar{e}_1 \\ \bar{e}_2 \\ \bar{e}_3 \end{Bmatrix} = \widetilde{\mathbf{G}}_1 \bar{u}_I + \xi_3 \widetilde{\mathbf{G}}_2 \bar{e}_I. \tag{41}$$

Similarly the other terms are as follows:

$$\frac{\partial u_I}{\partial \xi_2} = \widetilde{\mathbf{G}}_3 \bar{u}_I + \xi_3 \widetilde{\mathbf{G}}_4 \bar{e}_I, \tag{42}$$

$$\frac{\partial u_I}{\partial \xi_3} = \widetilde{\mathbf{G}}_5 \bar{e}_I. \tag{43}$$

The incremental gradient displacement ($\boldsymbol{\Omega}$) for non-linear part with Eq. (27) is as follows:

$$\Delta\boldsymbol{\Omega} = \begin{Bmatrix} \frac{\partial \Delta u_1}{\partial \xi_1} \\ \frac{\partial \Delta u_2}{\partial \xi_1} \\ \frac{\partial \Delta u_3}{\partial \xi_1} \end{Bmatrix} = \begin{bmatrix} \widetilde{\mathbf{G}}_1 & \xi_3 \widetilde{\mathbf{G}}_2 \\ \widetilde{\mathbf{G}}_3 & \xi_3 \widetilde{\mathbf{G}}_4 \\ \mathbf{0} & \widetilde{\mathbf{G}}_5 \end{bmatrix} \begin{Bmatrix} \Delta \bar{u}_I \\ \Delta \bar{e}_I \end{Bmatrix} = \widetilde{\mathbf{G}} \begin{Bmatrix} \Delta \bar{\mathbf{u}} \\ \Delta \boldsymbol{\theta} \end{Bmatrix} = \widetilde{\mathbf{G}} \Delta \mathbf{U}. \tag{44}$$

Then incremental variation of the non-linear part of Green strain is as follows:

$$\delta(\Delta^{NL}\widetilde{E}) = \delta\Delta\mathbf{Q}\widetilde{\mathbf{G}}\Delta\mathbf{U}. \tag{45}$$

Substituting the non-linear part of strain into Eq. (37), the following geometric stiffness matrix is obtained.

$$\int S_{\alpha\beta}\delta(\Delta^{NL}\widetilde{E})\,\mathrm{d}V = \int \delta(\Delta^{NL}\widetilde{E})^{\mathrm{T}} S_{\alpha\beta}\,\mathrm{d}V = \int \delta\Delta\boldsymbol{\Omega}^{\mathrm{T}}\Delta\mathbf{Q}^{\mathrm{T}} S_{\alpha\beta}\,\mathrm{d}V. \tag{46}$$

The geometric stiffness matrix in the natural coordinate is analytically integrated through the thickness. By the transformation the natural to the global frame, the element geometric stiffness matrix is obtained on the global frame with 6×6 sub-matrix.

$$[\mathbf{K}_{\mathbf{G}}] = \int \begin{bmatrix} \mathbf{K}_{\mathbf{G}}^{\mathbf{11}} & \mathbf{K}_{\mathbf{G}}^{\mathbf{12}} \\ \mathbf{K}_{\mathbf{G}}^{\mathbf{21}} & \mathbf{K}_{\mathbf{G}}^{\mathbf{22}} \end{bmatrix}_{6\times 6} \mathrm{d}A, \tag{47}$$

where the sub-matrix of $[\mathbf{K}_{\mathbf{G}}]$ is shown in Han et al. (2004). Then the final assembled incremental non-linear equilibrium equation can be written is

$$([\mathbf{K}_{\mathbf{L}}] + [\mathbf{K}_{\mathbf{G}}])\Delta\mathbf{u} = {}^{t+\Delta t}\bar{\mathbf{F}} - \mathbf{F}, \tag{48}$$

where $\bar{\mathbf{F}}$ and $\mathbf{F}$ are the external and internal forces respectively.

The equilibrium equation must be satisfied throughout the complete history of loading and the non-linear processing will be stopped only when the out of balance forces are negligible within a certain convergence limit. If it is necessary to extend the stability analysis beyond the limit point, i.e. in the so-called postbuckling range, appropriate solution procedures must be applied. One approach is to use the arc-length control method in conjunction with the Newton–Raphson method to extend the stability analysis beyond the limit point, by Crisfield (1981).

8. Numerical examples

The present nine-node assumed strain shell element is implemented in the extended version of the FEAP (Zienkiewicz and Taylor (1989, 2000)). In order to validate this present shell element, several numerical examples are solved to test the performance of the shell element in static analysis. Examples are anisotropic composite materials for the comparisons and further developments. Before proceeding with the following study, the influence of the finite element mesh is quantified. As a result of the mesh convergence study shown in Tables 1(a) and 1(b). Full plate is analyzed with various mesh sizes (Fig. 7). The boundary condition is simply supported and the geometry and material properties are as follow:

$$E_1/E_2 = 40, \quad G_{12} = G_{13} = 0.6E_2, \quad G_{23} = 0.5E_2, \quad v_{12} = 0.25, \quad a/h = 10, \quad a = 10, \quad q = 1.0. \tag{49}$$

The results are presented in the non-dimensional form using the equation:

$$\bar{w} = w \times \frac{E_2 h^3}{q a^4} \times 10^3. \tag{50}$$

The results using a regular mesh show an excellent correlation to the results given by Reddy (1997).

Table 1(a)
Non-dimensional displacement of composite plates (cross-ply)

Mesh	0/90	0/90/0	0/90/90/0	0/90/0/90
2×2	14.077	7.163	6.856	7.057
4×4	14.014	6.926	6.690	6.931
8×8	14.054	6.919	6.682	6.925
10×10	14.059	6.919	6.682	6.925
FSDT[a]	14.069	6.919	6.682	6.926

[a] Reissner–Mindlin thick-plate theory solution, First order Shear Deformation Theory (Reddy, 1997).

Table 1(b)
Non-dimensional displacement of composite plates ($\theta/-\theta/\theta/-\theta$)

Mesh	5	15	30	45
2×2	7.039	6.287	4.958	4.536
4×4	6.740	6.085	4.827	4.429
8×8	6.741	6.086	4.825	4.426
10×10	6.741	6.086	4.825	4.426
FSDT[a]	6.741	6.086	4.825	4.426

[a] Reissner–Mindlin thick-plate theory solution, First order Shear Deformation Theory (Reddy, 1997).

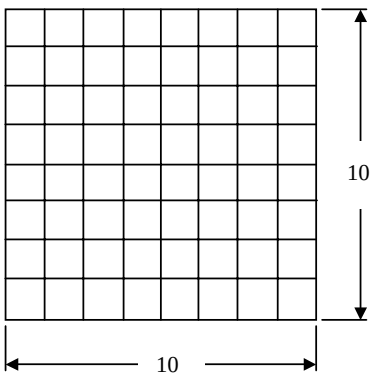

Fig. 7. Meshes for simply supported composite plate.

In order to validate the FEM code developed for geometrically nonlinear analysis, the load-deflection curve at center of a laminated composite plate with sixteen layers is computed and compared with the results reported by Saigal et al. (1986) and Lee and Kanok-Nukulchai (1998). The side length of the square plate model is $a = 254$ mm, the total thickness of the laminated composite plate is $h = 2.114$ mm, and all layers have the same thickness of $h/16$, respectively. The material properties used are $E_1 = 13.1 \times 10^4$ N/mm^2; $E_2 = E_3 = 1.303 \times 10^4$ N/mm^2; $G_{12} = G_{13} = 0.641 \times 10^4$ N/mm^2; $G_{23} = 0.4721 \times 10^4$ N/mm^2; $v_{12} = v_{23} = v_{13} = 0.38$ and the laminate has the fiber angle of $(45^\circ/-45^\circ/0^\circ_2/45^\circ/-45^\circ/90^\circ_2)_s$ in which the subscript s denotes symmetry. The plate with all clamped boundary edges is subjected to a uniformly distributed load. The full plate with a 4×4 mesh is used in this analysis. For 20 equal load increments, the standard NR method is used in this example. Fig. 8 shows good agreement with the solutions reported by Saigal et al. (1986) and Lee and Kanok-Nukulchai (1998).

The finite element formulation described earlier is now implemented to study the influences of shear and combination of in-plane shear, compression and lateral loading on the postbuckling analysis of a variety of laminated composite plates. Fig. 9 shows the dimensions and coordinates of a laminated composite plate

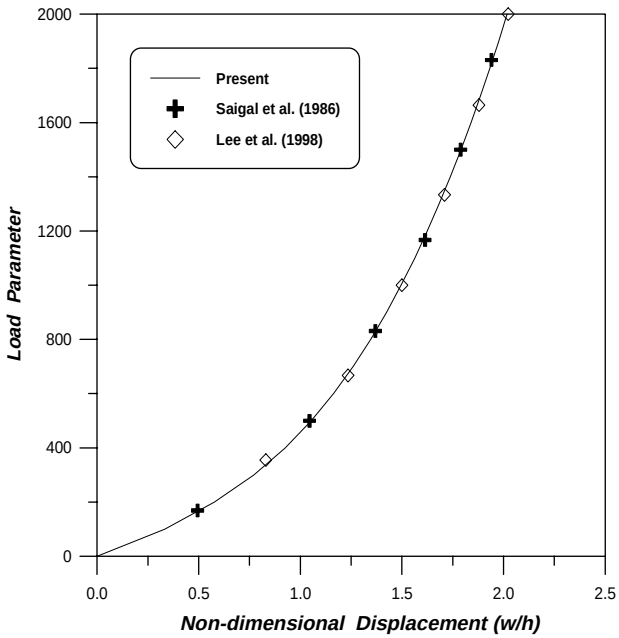

Fig. 8. Load deflection curve of center deflection.

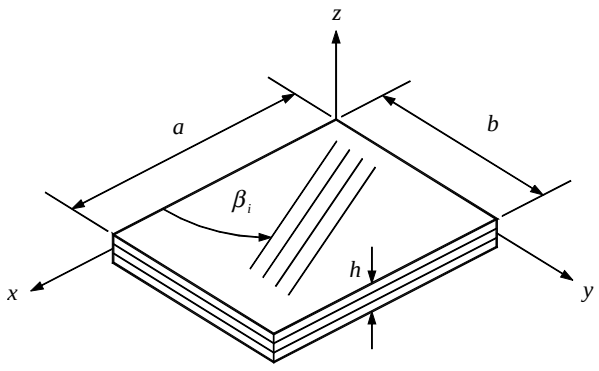

Fig. 9. Geometry of laminated composite plates ($a = b = 250$ mm, $h = 2.5$ mm).

Table 2
Material properties (GPa)

Material	E_1	E_2	E_3	G_{12}	G_{23}	G_{13}	v_{12}	v_{23}	v_{13}
Boron/epoxy	206.9	20.7	20.7	5.2	5.2	5.2	0.3	0.3	0.3
Carbon/epoxy	206.9	5.2	5.2	2.6	2.6	2.6	0.25	0.25	0.25
Glass/epoxy	53.8	17.9	17.9	8.9	8.9	8.9	0.25	0.25	0.25

analyzed by the aforementioned theories for the materials whose properties are listed in Table 2. Figs. 10 and 11 also show the loading types of a laminated composite plate. Full plate is analyzed with 8×8 mesh sizes. Non-dimensional buckling load, lateral load and parameter are defined as $\overline{P} = \frac{Pb^2}{E_2h^3}$, $\bar{q} = \frac{qb^4}{E_2h^4}$ and $C_k = \frac{qb^2}{Ph}$, respectively.

8.1. Shear loading

Fig. 12 shows the non-dimensional buckling loads at bifurcation point of unidirectional composite plates under the positive and negative shears with clamped ends. The results used for comparison are mainly taken from the work of Zhang and Matthews (1983a,b, 1985). These are based on energy methods using beam eigenfunctions, with the transverse shear deformations ignored. As expected, the results obtained from this study are in good agreement with those reported by Zhang and Matthews. It can be also observed from the figure that the critical loads of the composite plate under the negative shear are higher than those of the positive shear for all fiber angles. This can be explained by the fact that the compression occurred by the negative shear increases the stiffness in the fiber orientation. Note that the buckling load in the case is heavily dependent on

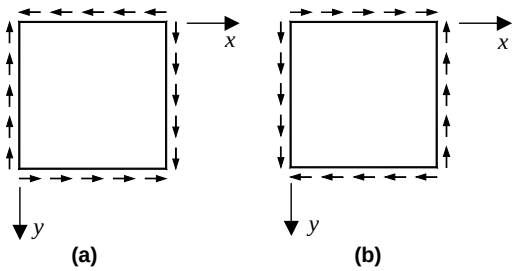

Fig. 10. Positive and negative shear loading of a laminated composite plate: (a) positive, (b) negative.

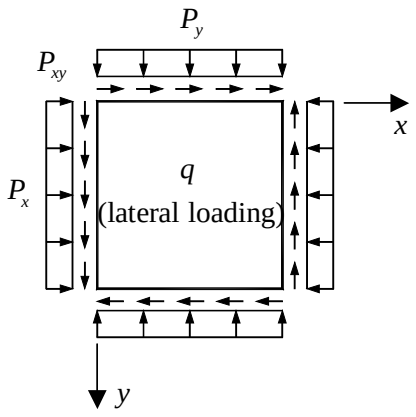

Fig. 11. Shear, compression and lateral loading of a laminated composite plate.

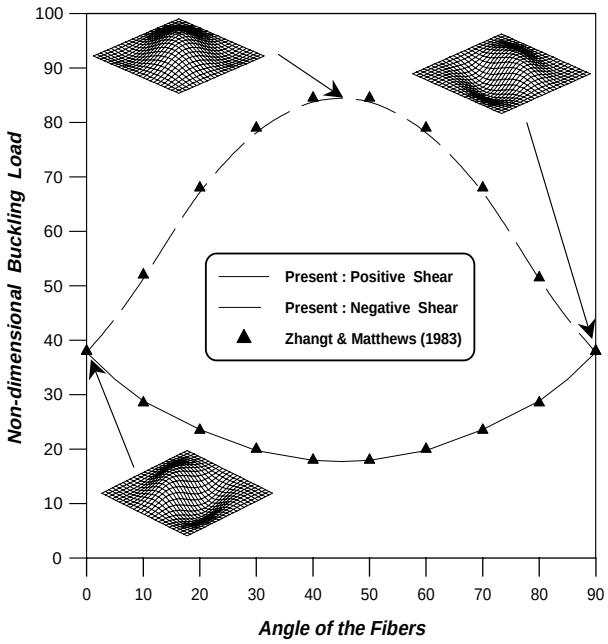

Fig. 12. Square laminated composite plate with unidirectional lay-up; critical shear load with fiber angle, boron/epoxy, $(\theta)_{20}$.

the fiber orientation. Among these, the buckling load of composite plate with the fiber angle of 45° exhibits the highest value.

Fig. 13 shows central deflections of square composite plates under the increased shear loads after initial buckling. The boron/epoxy composites are used and all edges of the plate are simply supported. For a plate with four numbers of alternate layers, the postbuckling paths show similar trends regardless of the fiber angles and direction of the applied shears. However, it can be observed that the induced deflection amplitude of the

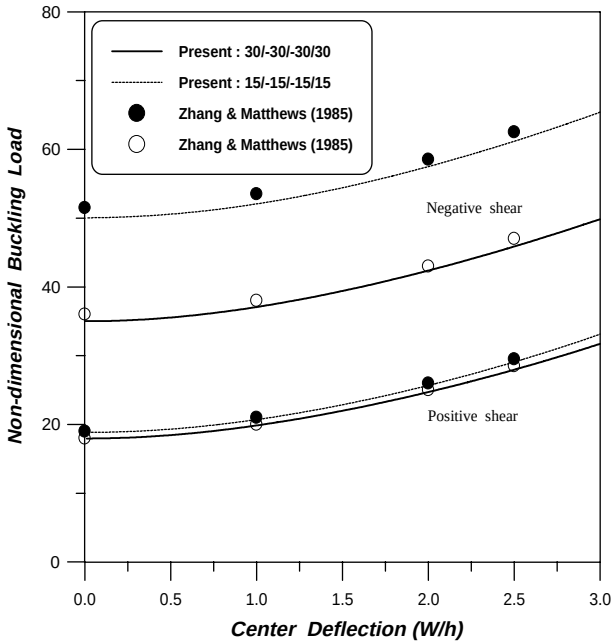

Fig. 13. Shear loading–central deflection relations of square boron/epoxy plates; different fiber angles.

[30/−30/−30/30] laminate is significantly higher than that of [15/−15/−15/15]. Even for the same fiber orientation, the difference becomes more dramatic for the case of different number of layers (two and four layers) shown in Fig. 14. This observation provides us with a clue that it could be better to use large number of alternate layers in designing a lay-up sequence especially when the negative shear is applied. In this case, big ply angles and large number of layers result in better rigidity against shear loading.

In Fig. 15, it is shown that the center deflection of anti-symmetric laminated composite plates subjected to the pure shear loading for the different fiber angles. It may be noticed that the load-deflection curve of composite plate with the fiber angle of [45/−45/45/−45] exhibits the higher value than others by $10 \sim 30\%$.

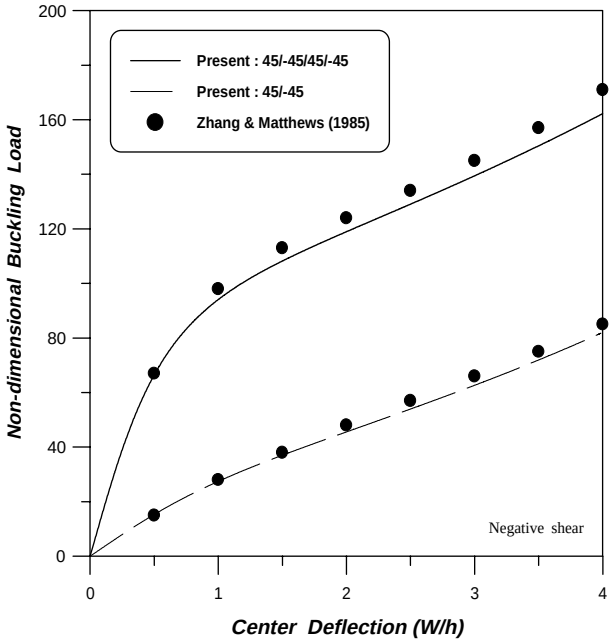

Fig. 14. Variation of central deflection with applied shear of carbon/epoxy plates; anti-symmetric lay-up.

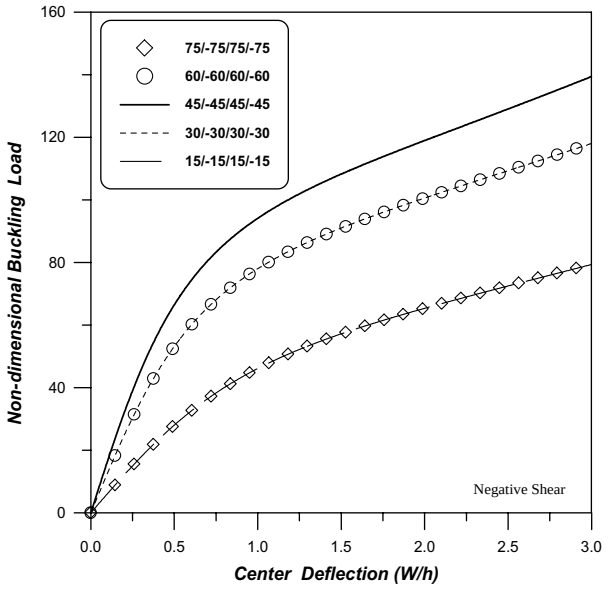

Fig. 15. Variation of central deflection with applied shear of carbon/epoxy plates; anti-symmetric lay-up.

8.2. Combination of in-plane shear and lateral loading

Fig. 16 shows the variation of central deflection of the [45/−45/−45/45] composite plate under the combination of in-plane shear and lateral loading ($C_k \neq 0$). The edges of the laminated composite plates are

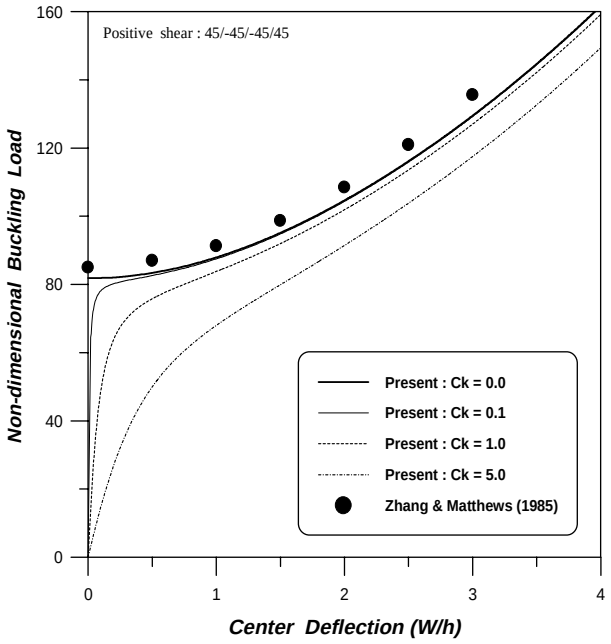

Fig. 16. Variation of central deflection with loading of square carbon/epoxy plates; symmetric lay-up, under the combination of in-plane shear and lateral loading.

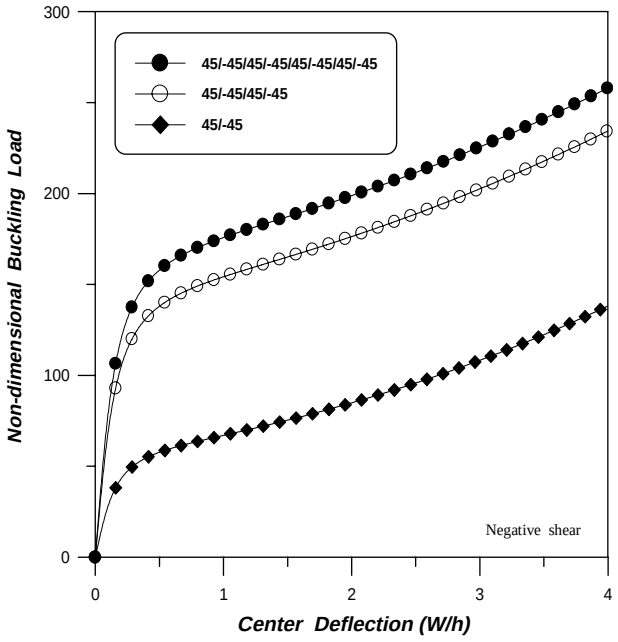

Fig. 17. Variation of central deflection with loading of square carbon/epoxy plates; anti-symmetric lay-up, under the combination of in-plane shear and lateral loading ($C_k = 1.0$).

considered to be loosely clamped that in-plane stresses are zero but deflection and rotation are restrained on the boundaries. As the parameter C_k increases, the deflections of the plate increase. It is predictable because it is expected that an increased lateral loading ratio results in larger deflection for increased buckling load. For the same ply orientation, Fig. 17 shows the influence of number of layers on the load-central deflection of

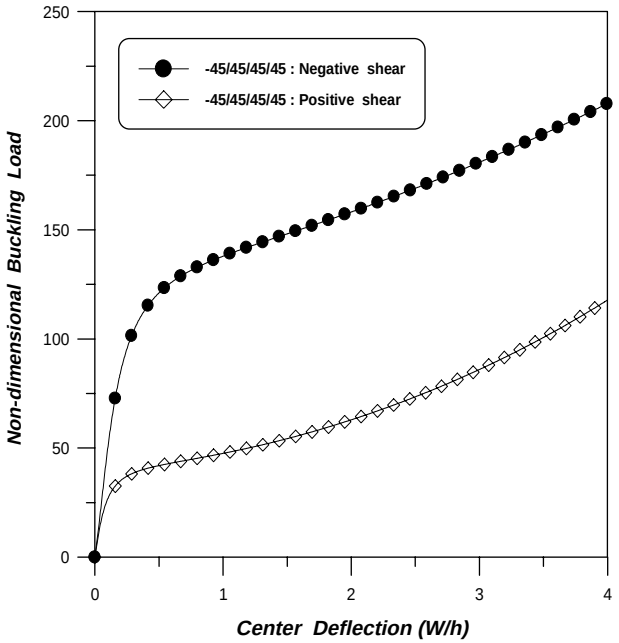

Fig. 18. Variation of central deflection with loading of square carbon/epoxy plates; asymmetric lay-up, under the combination of in-plane shear and lateral loading ($C_k = 1.0$).

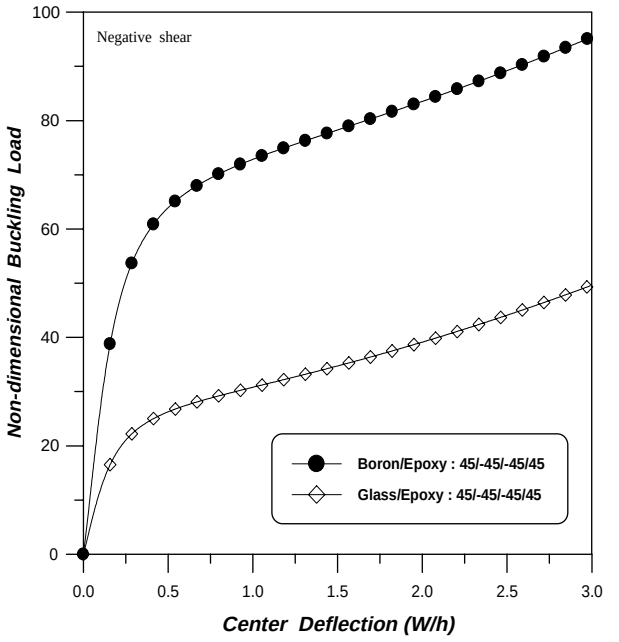

Fig. 19. Variation of central deflection with loading of square plates made of different materials; symmetric lay-up, under the combination of in-plane shear and lateral loading ($C_k = 1.0$).

plates under the combination of in-plane shear and lateral loading ($C_k = 1.0$). For the fiber angle of 45°, the central deflections for the four and eight number of layers are close to each other. On the other hand, the induced deflection for the two numbers of layers is extremely higher than others. It may be also noted that the directions of applied shear are negligible due to anti-symmetric lay-up sequences. By contrast, for the asymmetric case shown in Fig. 18, the load-central deflection curves are significantly different for different

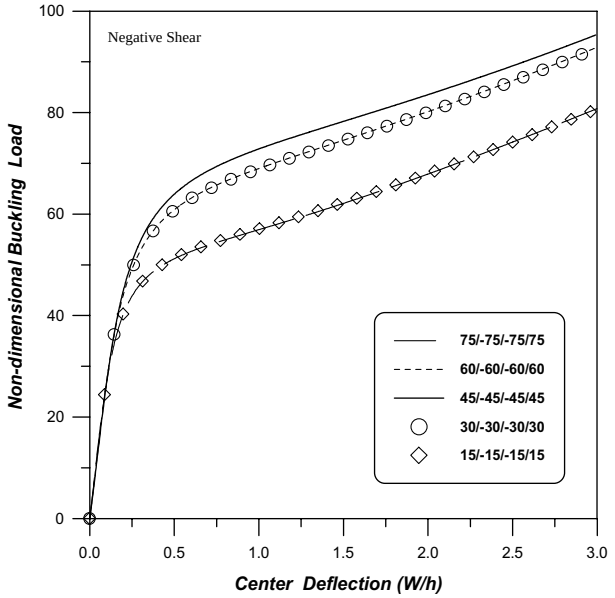

Fig. 20. Variation of central deflection with loading of square boron/epoxy plates; symmetric lay-up, under the combination of in-plane shear and lateral loading ($C_k = 1.0$).

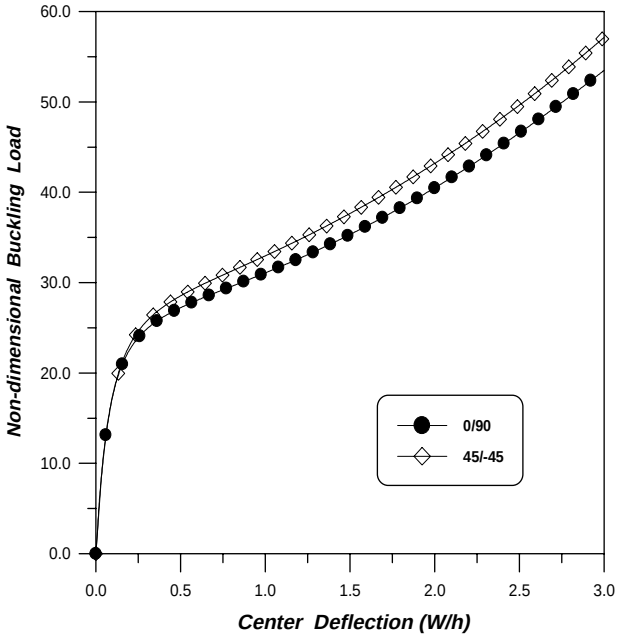

Fig. 21. Variation of central deflection with loading of square carbon/epoxy plates; anti-symmetric lay-up, under the combination of in-plane shear, compression and lateral loading ($C_k = 1.0$, $P_x + P_{xy} + q$).

directions of the shear. Moreover, Fig. 19 shows the dramatic variation of central deflection with loading of square symmetric laminates made of different materials (Boron/Epoxy and Glass/Epoxy). Fig. 20 shows the center deflection of symmetric laminated composite plates subjected to the in-plane shear and lateral loading for the different fiber angles. As expected, the load-deflection curve of composite plate with the fiber angle of

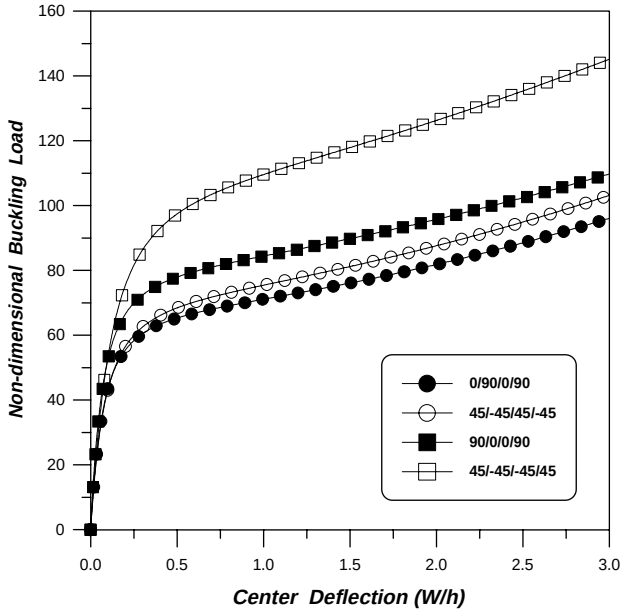

Fig. 22. Variation of central deflection with loading of square carbon/epoxy plates; under the combination of in-plane shear, compression and lateral loading ($C_k = 1.0$, $P_x + P_{xy} + q$).

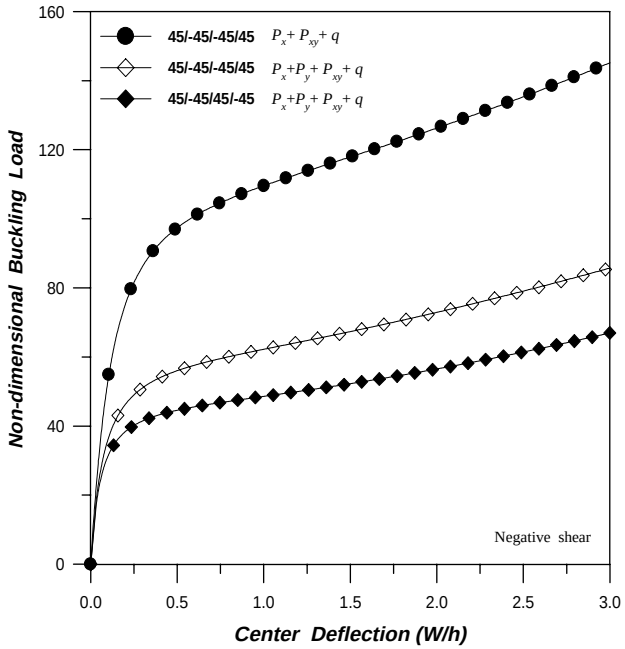

Fig. 23. Variation of central deflection with loading of square carbon/epoxy plates; under the combination of in-plane shear, compression and lateral loading ($C_k = 1.0$).

[45/−45/−45/45] exhibits the highest value. However, the difference decreases when compared with the case of shear loading as shown in Fig. 15. From Fig. 21, we can also observe similar trend for the fiber angles of [0/90] and [45/−45]. From the observations, it may be noticed that the coupling effects of in-plane shear and lateral loading makes deleterious contributions to the buckling loads of composite plates for the different fiber angles.

Fig. 22 shows the difference of behaviors between anti-symmetric orthotropy and angle-ply laminates made of same material (Carbon/Epoxy). It can be observed from the figures that the buckling load of

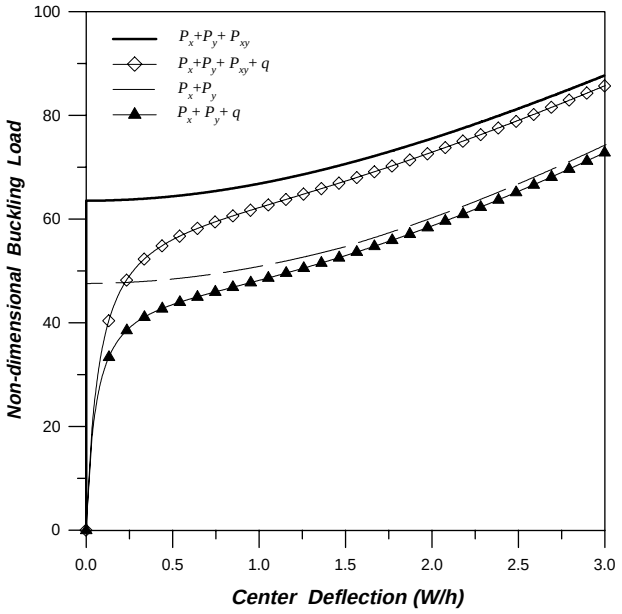

Fig. 24. Variation of central deflection with loading of square carbon/epoxy plates; symmetric lay-up (45/−45/−45/45), under the combination of in-plane shear, biaxial compression and lateral loading ($C_k = 1.0$).

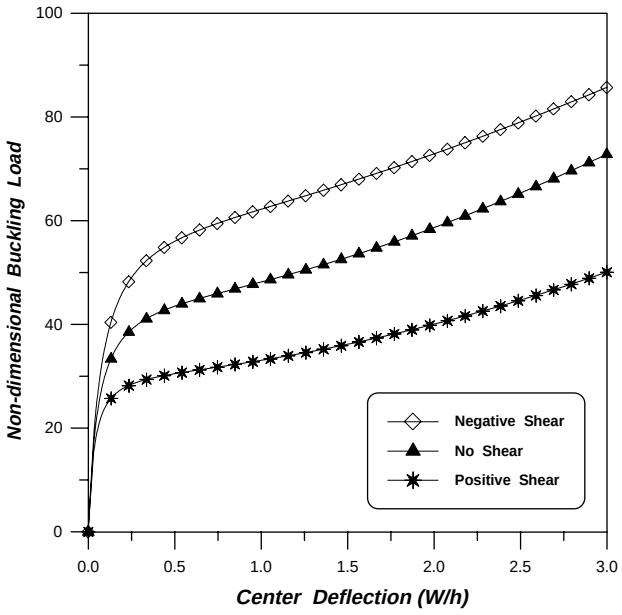

Fig. 25. Variation of central deflection with loading of square carbon/epoxy plates; symmetric lay-up (45/−45/−45/45), under the combination of in-plane shear, biaxial compression and lateral loading ($C_k = 1.0$, $P_x + P_y + P_{xy} + q$).

[45/−45/−45/45] laminate is higher than the others. We can also notice that the buckling load for angle-ply laminates is higher than that of orthotropic laminates. For the fiber angle of 45°, Fig. 23 shows buckling loads of the plate subjected to action of in-plane compressive loads (P_x and P_y), shear load (P_{xy}), and lateral load (q). It can be also observed from the figures that the buckling load of [45/−45/−45/45] laminate is higher than the case of [45/−45/45/−45]. The parametric case studies reveal the importance of lay-up sequences for efficient and economic design of composite plates under the combined loading.

Figs. 24 and 25 show the buckling loads of [45/−45/−45/45] laminates subjected to different kinds of loading. The Fig. 24 shows how the deflection at the center of the plates varies with increasing shear and in-plane compressive loads after bifurcation point. Also, it can be seen that there are two postbuckling paths for each plate when the lateral loads are included. In Fig. 25, the effect of the applied shear directions in the plate with in-plane compressive and lateral loads is shown. These behaviors lead us to a conclusion that the influence of applied shear directions played a role in increasing or decreasing buckling loads.

9. Summary and conclusion

An intuitive prediction of the geometrically nonlinear behavior of laminated composite structures under combined loads is difficult because of their complexity and the combined effect of anisotropy, nonlinear geometry, and load condition. In this study, the postbuckling characteristics are analyzed by considering various parameters. The advanced finite element nonlinear analysis based on the Element-based Largrangian formulation shows the significance of stacking sequences and loading conditions for composite plates. From the parametric case studies, we find the following key observations in designing laminated composite structures.

1. The critical buckling loads of the composite plate under the negative shear are higher than those of the positive shear for all fiber angles. The buckling load in the case is heavily dependent on the fiber orientation. For shear loading, it is desirable to use fiber angle of 45°.
2. Even for the same fiber orientation, the difference of buckling loads becomes more dramatic for the case of different number of layers. In this case, big ply angles and large number of layers result in better rigidity against shear loading.
3. For plates subjected to the pure shear loading and the combination of in-plane shear and lateral loading, the directions of applied shear are negligible due to anti-symmetric lay-up sequences. By contrast, for the symmetric and the asymmetric case, the load-central deflection curves are significantly different for different directions of the shear.
4. We find that the buckling load for angle-ply laminates with fiber angle of 45° subjected to the combined loading is higher than that of orthotropic laminates. However, it may be noted that the influence of the combined loading on buckling loads for different fiber angles is smaller than that of single negative shear loading. In addition, the influence of applied shear directions increased or decreased the buckling loads of laminated composite plates with the combination of in-plane shear, compression and lateral loading.

The results of this study may serve as benchmark for future guidelines in designing laminated composite plates under the combination of in-plane shear, compression and lateral loading. But our parametric study is only an example and more studies should be carried out for individual cases.

Acknowledgement

The authors would like to express our profound gratitude to Prof. W. Kanok-Nukulchai in AIT and Dr. K.D. Kim in Konkuk Univ., Korea for their encouragement while preparing this paper.

References

Ahmad, S., Irons, B.M., Zienkiewicz, O.C., 1970. Analysis of thick and thin shell structures by curved finite elements. International Journal for Numerical Methods in Engineering 2, 419–451.

Belytschko, T., Wong, B.L., Stolarski, H., 1989. Assumed strain stabilization procedure for the 9-node lagrange shell element. International Journal for Numerical Methods in Engineering 28, 385–414.

Crisfield, M.A., 1981. A fast incremental/iterative solution procedures that handles snap-through. Computers and Structures 13, 55–62.

Featherston, C.A., Watson, A., 2005. Buckling of optimized flat composite plates under shear and in-plane bending. Composites Science and Technology 65 (6), 839–853.

Featherston, C.A., 2003. Imperfection sensitivity of curved panels under combined compression and shear. International Journal of Non-linear Mechanics 38 (2), 225–238.

Groesberg, S.W., 1968. Advanced Mechanics. Wiley, New York.

Han, S.C., Kim, K.D., Kanok-Nukulchai, W., 2004. An element-based 9-node resultant shell element for large deformation analysis of laminated composite plates and shells. Structural Engineering and Mechanics, An International Journal 18 (6), 807–829.

Huang, H.C., Hinton, E., 1986. A new nine node degenerated shell element with enhanced membrane and shear interpolation. International Journal for Numerical Methods in Engineering 22, 73–92.

Jang, J., Pinsky, P.M., 1987. An assumed covariant strain based 9-node shell element. International Journal for Numerical Methods in Engineering 24, 2389–2411.

Kanok-Nukulchai, W., 1979. A simple and efficient finite element for general shell analysis. International Journal for Numerical Methods in Engineering 14, 179–200.

Kim, K.D., Lomboy, G.R., Han, S.C., 2003. A co-rotational 8-node assumed strain shell element for postbuckling analysis of laminated composite plates and shells. Computational Mechanics 30 (4), 330–342.

Kim, K.D., Park, T.H., 2002. An 8-node Assumed Strain Element with Explicit Integration for Isotropic and Laminated Composite Shells. Structural Engineering and Mechanics 13, 387–410.

Kim, K.D., Voyiadjis, G.Z., 1999. Non-linear Finite Element Analysis of Composite Panels. Composites Part B: Engineering 30, 365–381.

Lee, S.J., Kanok-Nukulchai, W., 1998. A Nine-Node Assumed Strain Finite Element for Large Deformation Analysis of Laminated Shells. International Journal for Numerical Methods in Engineering 42, 777–798.

Loughlan, J., 2001. The shear buckling behaviour of thin composite plates with particular reference to the effects of bend-twist coupling. International Journal of Mechanical Sciences 43 (3), 771–792.

Meirovitch, L., 1970. Methods of Analytical Dynamics. McGraw-Hill, NewYork.

Reddy, J.N., 1997. Mechanics of Laminated Composite Plates. CRC Press, Florida.

Saigal, S., Kapania, R.K., Yang, Y.T., 1986. Geometrically nonlinear finite element analysis of imperfect laminated shells. Journal of Composite Materials 20, 197–214.

Shufrin, I., Eisenberger, M., 2005. Stability and vibration of shear deformable plates-first order and higher order analyses. International Journal of Solids and Structures 42, 1225–1251.

Simo, J.C., Hughes, T.J.R., 1986. On the variational formulations of assumed strain methods. Journal of Applied Mechanics, ASME 53, 51–54.

Wong, W.K., 1984. Pseudo Lagrangian Formulation for Large Deformation Analysis of Continua and Structures. Master Thesis, School of Civil Engineering, A.I.T.

Zhang, Y., Matthews, F.L., 1983a. Initial buckling of curved panels of generally layered composite materials. Composite Structures 1 (1), 3–30.

Zhang, Y., Matthews, F.L., 1983b. Postbuckling behaviour of curved panels of generally layered composite materials. Composite Structures 1 (2), 115–135.

Zhang, Y., Matthews, F.L., 1985. Large deflection behavior of simply supported laminated panels under in-plane loading. Journal of Applied Mechanics, ASME 52, 553–558.

Zienkiewicz, O.C., Taylor, R.L., 1989. The Finite Element Method. McGraw-Hill, London.

Zienkiewicz, O.C., Taylor, R.L., 2000. The Finite Element Method. Butterworth-Heinemann, London.